Probability distribution of internal stress in relaxed dislocation systems

Ferenc F. Csikor* and István Groma
Department of General Physics, Eötvös University Budapest, H-1518 Budapest, P.O.B. 32, Hungary
(Received 22 March 2004; published 18 August 2004)

The probability distribution of the internal shear stress generated by systems of straight, parallel edge dislocations is studied. The stress distribution functions of randomly distributed dipoles and walls are calculated analytically. The stress distribution function of relaxed systems is also calculated analytically assuming relaxed configurations to be made up of uncorrelated perfect dipoles and walls. The resulting relaxed stress distribution function is compared to numerical simulations.

DOI: 10.1103/PhysRevB.70.064106 PACS number(s): 61.72.Lk, 62.20.Fe, 62.20.Hg, 62.20.Mk

I. INTRODUCTION

In the last decade it has become a key issue to establish an appropriate scheme for the multiscale modeling of material properties. At the submicron level, the mechanical features of crystalline materials are mainly determined by the collective behavior of dislocations. So, to link the 10 nm-scale description, where one can actually "see" individual dislocations, to the micron-scale description, the statistical properties of dislocation ensembles need to be understood. This can help in establishing appropriate models for problems like dislocation pattern formation or size effects. Although quite a number of different analytical[1–5] and numerical[6–14] models have been suggested to establish the connection between the two length scales, most of them rely on assumptions closely related to the statistical properties of dislocation systems. One important example is the justification of gradient terms introduced heuristically in many nonlocal phenomenological continuum theories of plasticity.[5,15–19] As it was shown by Groma, Csikor, and Zaiser,[5] a gradient term can only be strictly justified if dislocation-dislocation correlations have a short range character.

The probability distribution of the internal stress created by dislocation systems is an important measure of the statistical properties of these systems. As it is explained in detail in this paper, the shape of the central part of the stress distribution function is determined by the correlation length of the dislocation system considered. So, e.g., if one creates a dislocation configuration by discrete dislocation dynamics simulation and would like to determine the correlation length, it is much more effective and precise to numerically calculate and analyze the internal stress distribution function than the pair correlation functions, that have a complicated radial and angular dependence. Certainly, the stress distribution function provides less information, but the accuracy of the obtained parameters is much higher.

Another important issue is the connection between the probability distribution of the internal stress and the shape of broadened x-ray Bragg peaks. The only difference between the two is that the second one measures the distribution of the strain instead of the stress. This means that the way the theoretical description of line broadening created by dislocations needs to be handled is precisely the same as the calculation of the probability distribution of the internal stress.[20,21] It can be stated that, apart from minor differences, x-ray line profile measurement offers a method for the experimental investigation of the internal strain (stress) distribution.

A further practical aspect of the problem is that the precise knowledge of the analytical form of the internal stress distribution is a key issue for the $\mathcal{O}(N)$ time complexity stochastic dislocation dynamics simulation method proposed earlier by Groma and Bakó.[22]

Since the time-scale of typical deformation experiments is orders of magnitudes longer than the time needed to achieve local equilibrium in dislocation systems, it is reasonable to assume local equilibrium everywhere in the entire sample during such experiments as well as during simulations of such experiments. For this reason, the goal of this paper is to properly describe the internal stress distribution of relaxed dislocation systems. To reduce the complexity of the problem, two-dimensional (2D) configurations of straight parallel edge dislocations lying in a single slip system were analyzed. The slip plane was chosen to be the xz plane with dislocations parallel to the z axis. It is known from numerical simulations (see e.g., Zaiser, Miguel, and Groma[23]) that the relaxed state of such systems is homogeneous and contains dipoles and walls. According to this, the aim of this paper is to describe the stress distribution function generated by these two short range correlation type objects. It is known, too, that both dipoles and walls are stable structures against small enough external stresses. The analysis of the stress distribution function in the stressed case will be published in another paper.

For the description of relaxed dislocation configurations, let us model the angular dependence of the pair correlation functions of the relaxed state with Dirac delta functions. That is, dipoles are supposed to make a 45° angle to the x axis and walls are supposed to be perfectly vertical. It is also supposed that all correlations of the order higher than two vanish. In the lack of external stress, the relaxed configurations are symmetrical to mirroring the dislocation Burgers vectors. Based on these, as a first step, the stress distribution contributions of uncorrelated, homogeneous, and symmetrical configurations of dislocations, dipoles, and walls are discussed. After that, for modeling the relaxed configurations mentioned above, these contributions are combined.

II. GENERAL FORM OF THE PROBABILITY DISTRIBUTION OF THE INTERNAL STRESS

Let us consider a planar arrangement of N pointlike objects positioned at $\boldsymbol{r}_i$, $i=1,\ldots,N$. The objects are similar apart from a sign $s_i=\pm 1$. The elastic shear stress field the ith object generates has the form

$$\tau_{\mathrm{obj}}^{s_i}(\boldsymbol{r}-\boldsymbol{r}_i)=s_i\tau_{\mathrm{obj}}(\boldsymbol{r}-\boldsymbol{r}_i), \tag{1}$$

where the actual $\boldsymbol{r}$ dependence of $\tau_{\mathrm{obj}}(\boldsymbol{r})$ is determined by the type of object considered. With this, the total internal shear stress field generated by the objects can be expressed as

$$\tau(\boldsymbol{r})=\sum_{i=1}^{N}\tau_{\mathrm{obj}}^{s_i}(\boldsymbol{r}-\boldsymbol{r}_i). \tag{2}$$

The goal of this section is to determine the $P_{\mathrm{obj}}(\tau,\boldsymbol{r})$ probability density of this stress field at an arbitrary position $\boldsymbol{r}$.

For the calculation of $P_{\mathrm{obj}}(\tau,\boldsymbol{r})$ Markoff's method[24] was applied, that has been successfully used, among others, to determine the first moment and the asymptotic behavior of the internal stress distribution for straight, parallel dislocations (see Groma and Bakó[22]). The problem can be rigorously formulated mathematically as to find the $P_{\mathrm{obj}}(\tau_0,\boldsymbol{r})d\tau_0$ probability of fulfilling the relation

$$\tau_0-\frac{d\tau_0}{2}<\tau(\boldsymbol{r})<\tau_0+\frac{d\tau_0}{2} \tag{3}$$

for arbitrary τ_0 values. By introducing the N particle distribution function $w_{\mathrm{obj}}^{s_1,\ldots,s_N}(\boldsymbol{r}_1,\ldots,\boldsymbol{r}_N)$, the stress distribution function can be expressed as

$$P_{\mathrm{obj}}(\tau_0,\boldsymbol{r})d\tau_0=\sum_{s_1}\cdots\sum_{s_N}\int d\boldsymbol{r}_1\cdots\int d\boldsymbol{r}_N w_{\mathrm{obj}}^{s_1,\ldots,s_N}(\boldsymbol{r}_1,\ldots,\boldsymbol{r}_N), \tag{4}$$

where the sums and integrals are taken only over that regions of the configuration space where the inequalities (3) are satisfied. By introducing the quantity

$$\Delta^{s_1,\ldots,s_N}(\boldsymbol{r}_1,\ldots,\boldsymbol{r}_N)=\begin{cases}1 & \text{whenever (3) holds,}\\ 0 & \text{otherwise,}\end{cases} \tag{5}$$

the sums and integrals in Eq. (4) can be extended to the entire $\{\pm 1\}^N\times\Re^{2N}$ space

$$P_{\mathrm{obj}}(\tau_0,\boldsymbol{r})d\tau_0=\sum_{s_1=\pm 1}\cdots\sum_{s_N=\pm 1}\int_{-\infty}^{\infty}d\boldsymbol{r}_1\cdots\int_{-\infty}^{\infty}d\boldsymbol{r}_N \times\Delta^{s_1,\ldots,s_N}(\boldsymbol{r}_1,\ldots,\boldsymbol{r}_N)w_{\mathrm{obj}}^{s_1,s_2,\ldots,s_N}(\boldsymbol{r}_1,\boldsymbol{r}_2,\ldots,\boldsymbol{r}_N). \tag{6}$$

As it has been shown by Markoff,[24] $\Delta^{s_1,\ldots,s_N}(\boldsymbol{r}_1,\ldots,\boldsymbol{r}_N)$ can be expressed as

$$\Delta^{s_1,\ldots,s_N}(\boldsymbol{r}_1,\ldots,\boldsymbol{r}_N)=\frac{1}{\pi}\int_{-\infty}^{\infty}\frac{\sin(\alpha q)}{q}\exp(\mathrm{i}\gamma q)dq, \tag{7}$$

where $\alpha=d\tau_0/2$ and $\gamma=\Sigma_{i=1}^{N}\tau_{\mathrm{obj}}^{s_i}(\boldsymbol{r}-\boldsymbol{r}_i)-\tau_0$. By combining Eqs. (6) and (7), the Fourier transform of $P_{\mathrm{obj}}(\tau_0,\boldsymbol{r})$ with respect to τ_0 has the form[22]

$$\ln[P_{\mathrm{obj}}(q,\boldsymbol{r})]=-\sum_{s_1=\pm 1}\int_{\Re^2}\rho_{\mathrm{obj}}^{s_1}(\boldsymbol{r}_1)B_{\mathrm{obj}}^{s_1}(\boldsymbol{r}-\boldsymbol{r}_1,q)d\boldsymbol{r}_1 +\frac{1}{2}\sum_{s_1=\pm 1}\sum_{s_2=\pm 1}\int_{\Re^4}d_{\mathrm{obj}}^{s_1,s_2}(\boldsymbol{r}_1,\boldsymbol{r}_2) \times B_{\mathrm{obj}}^{s_1}(\boldsymbol{r}-\boldsymbol{r}_1,q)B_{\mathrm{obj}}^{s_2}(\boldsymbol{r}-\boldsymbol{r}_2,q)d\boldsymbol{r}_1d\boldsymbol{r}_2+\cdots, \tag{8}$$

where

$$B_{\mathrm{obj}}^{s}(\boldsymbol{r},q)=1-\exp[\mathrm{i}q\tau_{\mathrm{obj}}^{s}(\boldsymbol{r})], \tag{9}$$

$\rho_{\mathrm{obj}}^{s_1}(\boldsymbol{r}_1)$ denotes the density of objects with sign s_1 at position $\boldsymbol{r}_1$ and $d_{\mathrm{obj}}^{s_1,s_2}(\boldsymbol{r}_1,\boldsymbol{r}_2)$ is the pair correlation function of objects with signs s_1 and s_2.

In the rest of this paper, the expression of $P_{\mathrm{obj}}(q,\boldsymbol{r})$ in Eq. (8) is always used under the following simplifying conditions:

(1) The spatial arrangement of objects is assumed to be homogeneous and uncorrelated. This yields that only the first term of Eq. (8) is nonzero and the spatial dependence of ρ_{obj}^{s} vanishes.

(2) The configuration of objects is symmetrical with respect to the inversion of signs, leading to the disappearance of the imaginary part of Eq. (8).

Let us call object configurations fulfilling these conditions uncorrelated, homogeneous and symmetrical (UHS) systems. For UHS systems, Eq. (8) simplifies to

$$\ln[P_{\mathrm{obj}}^{\mathrm{UHS}}(q)]=-\rho_{\mathrm{obj}}\int_{\Re^2}\{1-\cos[q\tau_{\mathrm{obj}}(\boldsymbol{r})]\}d\boldsymbol{r}, \tag{10}$$

where $\rho_{\mathrm{obj}}=\rho_{\mathrm{obj}}^{-1}+\rho_{\mathrm{obj}}^{+1}$ is the total object density and $\tau_{\mathrm{obj}}(\boldsymbol{r})$ is the stress field of an individual object without the sign factor [cf. Eq. (1)]. It should be noted that $P_{\mathrm{obj}}^{\mathrm{UHS}}(q)$ in Eq. (10) is a real, even function of q, meaning that the UHS stress distribution function $P_{\mathrm{obj}}^{\mathrm{UHS}}(\tau)$ is real and even as well.

It needs to be mentioned at this point that, as it is explained in details by Groma and Bakó,[22] for individual dislocations the correlation effects always need to be taken into account in order to avoid crystal size dependence. However, for dislocation dipoles or multipoles considered in this paper, neglecting the correlations between these objects does not lead to such artificial effects.

For our further considerations, it is important to analyze the behavior of the stress distribution function $P_{\mathrm{obj}}^{\mathrm{UHS}}(\tau)$ at the simultaneous presence of multiple mutually independent UHS object populations $\mathrm{obj}_1,\ldots,\mathrm{obj}_M$. For such a case, the elastic shear stress field of the combined population is the sum of the stress fields of individual populations. As it is well known, the probability distribution of the sum of mutually independent probabilistic variables is the convolution of the individual probability distributions that is equivalent to a multiplication in the Fourier space. Thus, the stress distribution of the combined object configuration can be expressed as

$$\ln[P_{\mathrm{obj}}^{\mathrm{UHS}}(q)]=\sum_{j=1}^{M}\ln[P_{\mathrm{obj}_j}^{\mathrm{UHS}}(q)]. \tag{11}$$

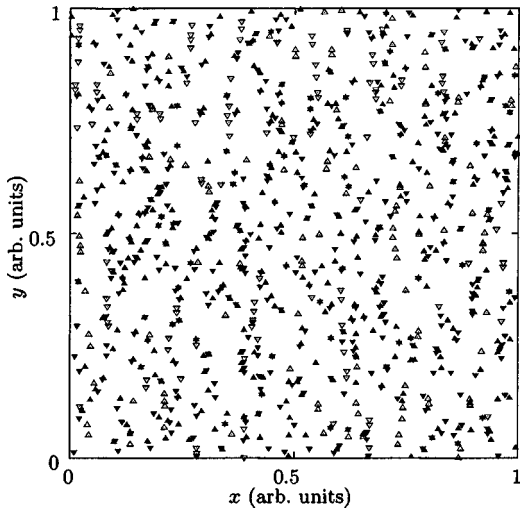

FIG. 1. Relaxed configuration of an initially random arrangement of 512 positive sign (upward triangles) and 512 negative sign (downward triangles) edge dislocations (the Burgers vectors are parallel to the *x* axis). Dislocations with an opposite-sign nearest neighbor are denoted by filled symbols (representing dipoles and standalone dislocations), the remaining dislocations are denoted by open symbols (walls and further standalone dislocations). Note the dominant presence of dipoles and walls.

III. STRESS DISTRIBUTION OF RELAXED CONFIGURATIONS OF STRAIGHT, PARALLEL EDGE DISLOCATIONS

In order to get a picture about relaxed dislocation configurations, numerical discrete dislocation dynamics simulations have been performed with the geometry described in Sec. I. The simulations were done with dimensionless variables. A unit square geometry with periodic boundary conditions was used to get rid of surface artifacts. Dislocation pair interactions were calculated using a high enough number of image dislocations (transposed by integer multiples of the two unit vectors parallel to the square edges) to get a smooth pair interaction function at the simulation square edges. Dislocation velocities were taken proportional to the net interaction stress of the other dislocations. No dislocation multiplication or annihilation was allowed. For numerical integration an adaptive step-size 4.5th order Runge–Kutta–Fehlberg method was used.

Figure 1 shows a representative equilibrium dislocation configuration obtained from an initially random distribution of an equal number of positive and negative sign edge dislocations with Burgers vectors parallel to the *x* axis, using the simulation method outlined above. As it can be seen, the relaxed state can be described as an array of dipoles and walls. The dipole angles are very close to the unstressed 45° value and the walls are nearly straight and vertical, i.e., it is a good approximation to assume that these structures are independent of each other. The relaxation process can be viewed as a relatively fast formation of dipoles and walls followed by an extremely slow rearrangement of these objects.

According to the above, in the following the stress distribution functions created by individual dislocations and UHS configurations of dipoles and walls are analyzed. At the end of this section, all these are combined into a model of the stress distribution function of relaxed dislocation configurations.

A. Individual dislocations

The stress field of a straight, infinite edge dislocation parallel to the *z* axis sliding in the *xz* plane has the form[30]

$$\tau^{s}_{\mathrm{dis}}(\boldsymbol{r}) = s\tau_{\mathrm{dis}}(\boldsymbol{r}) = sbG\frac{x(x^2-y^2)}{(x^2+y^2)^2} = \frac{sK(\varphi)}{r}, \qquad (12)$$

where b is the absolute value of the Burgers vector and G is a combination of the elastic moduli.[25] It is worth mentioning that the last form of the stress field is applicable to any dislocation type by using an appropriate $K(\varphi)$, thus the following results written in this form are valid for any type of straight dislocations.

The stress distribution function of straight, parallel dislocation systems was analyzed in detail by Groma and Bakó.[22] In that work, only those properties of the stress distribution function were considered that depend only on the properties of individual dislocations. Using Markoff's method described in the previous section, it was found that for *any* dislocation configuration the stress distribution function asymptotically decays as

$$P_{\mathrm{dis}}(\tau,\boldsymbol{r}) \to C\rho_{\mathrm{dis}}(\boldsymbol{r})\frac{1}{|\tau|^3}, \quad \text{whenever } |\tau| \to \infty, \qquad (13)$$

where $\rho_{\mathrm{dis}}(\boldsymbol{r})$ is the dislocation density (the number of dislocations intersecting a surface unit) at position $\boldsymbol{r}$ and

$$C = \tfrac{1}{2}\int_0^{2\pi} K^2(\varphi)d\varphi \qquad (14)$$

is the "contrast factor" of the dislocation type considered. For edge dislocations, $C=(\pi/4)(Gb)^2$. It is important to note that the asymptotic behavior given by Eq. (13) depends only on the local properties of the dislocation system, irrespective of the actual arrangement. In other words this means that the high stresses come entirely from the diverging stress field near the dislocation positions.

For dislocation systems homogeneous on the length scale of the average dislocation spacing, Eq. (13) can be written as

$$P^{\mathrm{H}}_{\mathrm{dis}}(\tau) \to C\rho_{\mathrm{dis}}\frac{1}{|\tau|^3}, \quad \text{whenever } |\tau| \to \infty. \qquad (15)$$

In the Fourier space, this leads to the formula[22]

$$\ln[P^{\mathrm{H}}_{\mathrm{dis}}(q)] \to C\rho_{\mathrm{dis}}q^2\ln\left(\frac{|q|}{q_{\mathrm{eff}}}\right), \qquad (16)$$

whenever $|q|\to 0$, where q_{eff} is an unknown parameter depending on the characteristic length scale of the dislocation assembly (e.g., crystal size, correlation length, or dipole size).

B. Monodisperse ideal dipoles

In the following, a dipole characterized by an infinitesimally small size but finite dipole moment is referred to as an

ideal dipole. Such a dipole can be treated as a pointlike object. A real dipole can be approximated by an ideal one if its size is less than the length scale of interest. In a similar way as in electrostatics, the stress field of an ideal dislocation dipole can be expressed as

$$\tau^{s}_{\mathrm{idip}}(\boldsymbol{r}) = s\,\tau_{\mathrm{idip}}(\boldsymbol{r}) = s\boldsymbol{p}\frac{d\tau_{\mathrm{dis}}(\boldsymbol{r})}{d\boldsymbol{r}}, \tag{17}$$

where the dipole vector $\boldsymbol{p}$ (the relative position vector connecting the negative constituent dislocation to the positive one) is chosen to point rightwards, $\arg(\boldsymbol{p}) \in [-\pi/2, \pi/2)$. Together with the sign $s = \pm 1$, this choice unambiguously describes all possible dipole orientations. Performing the differentiation in Eq. (17) leads to

$$\tau_{\mathrm{idip}}(\boldsymbol{r}) = \frac{L(\varphi)}{r^2}, \tag{18}$$

where

$$L(\varphi) = -|\boldsymbol{p}|\left[K(\varphi)\cos(\varphi_{\mathrm{rel}}) + \frac{dK(\varphi)}{d\varphi}\sin(\varphi_{\mathrm{rel}})\right] \tag{19}$$

is a trigonometric polynomial and $\varphi_{\mathrm{rel}} = \varphi - \arg(\boldsymbol{p})$.

By substituting Eq. (18) into Eq. (10), one obtains that for UHS ideal dipole systems the stress distribution function is

$$\ln[P^{\mathrm{UHS}}_{\mathrm{idip}}(q)] = -\rho_{\mathrm{idip}}\int_0^{2\pi} d\varphi \int_0^{\infty} r dr\left[1 - \cos\left(\frac{qL(\varphi)}{r^2}\right)\right], \tag{20}$$

where ρ_{idip} is the density of ideal dipoles. With the variable substitution $x = |qL(\varphi)|/r^2$, the integral with respect to x can be performed analytically, leading to

$$\ln[P^{\mathrm{UHS}}_{\mathrm{idip}}(q)] = -D\rho_{\mathrm{idip}}|q|, \tag{21}$$

where

$$D = \frac{\pi}{4}\int_0^{2\pi} |L(\varphi)| d\varphi. \tag{22}$$

Since the order of the trigonometric polynomial $L(\varphi)$ is usually higher than four, the value of D can only be calculated numerically. For 45° edge dislocation dipoles, $D \approx 3.55bG|\boldsymbol{p}|$.

Equation (21) means that the stress distribution function created by ideal dipoles is *Lorentzian* with a half width of $D\rho_{\mathrm{idip}}$. (For x-ray line profiles, the Lorentzian character has been already obtained by Krivoglaz[26] but without the explicit expression of the half width.)

C. Monodisperse "real" dipoles

In contrast to ideal dipoles considered in the previous section, in real systems dipoles always have a finite size. Consequently, the stress field of a real dipole,

$$\tau^{s}_{\mathrm{rdip}}(\boldsymbol{r}) = s\,\tau_{\mathrm{rdip}}(\boldsymbol{r}), \tag{23}$$

is characterized by the asymptotes

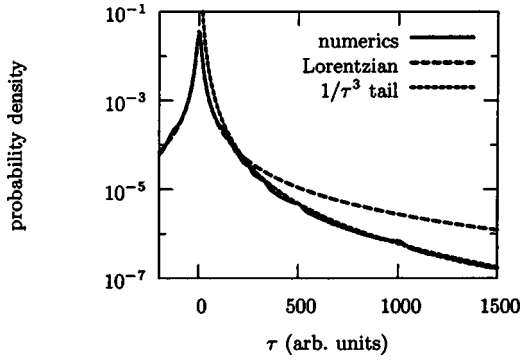

FIG. 2. Numerically obtained stress distribution function of a random dipole system and the analytically known Lorentzian and $1/\tau^3$ asymptotes. For the numerics, dipoles of eight different sizes were used, each of which is represented by a small peak on the numerical curve. In the case of smooth dipole size distributions the peaks get blurred and eventually disappear (see Fig. 5), that is why they are omitted from the present analysis.

$$\tau_{\mathrm{rdip}}(\boldsymbol{r}) \to \begin{cases} \tau^{+1}_{\mathrm{dis}}\left(\boldsymbol{r} - \frac{1}{2}\boldsymbol{p}\right), & \text{whenever } \left|\boldsymbol{r} - \frac{1}{2}\boldsymbol{p}\right| \to 0, \\ \tau^{-1}_{\mathrm{dis}}\left(\boldsymbol{r} + \frac{1}{2}\boldsymbol{p}\right), & \text{whenever } \left|\boldsymbol{r} + \frac{1}{2}\boldsymbol{p}\right| \to 0, \\ \tau_{\mathrm{idip}}(\boldsymbol{r}), & \text{whenever } |\boldsymbol{r}| \to \infty, \end{cases} \tag{24}$$

where τ_{dis} denotes the stress field of an individual dislocation [Eq. (12)] and τ_{idip} is the stress field of ideal dipoles given by Eq. (18). $\tau_{\mathrm{rdip}}(\boldsymbol{r})$ smoothly interpolates between these regimes.

The complicated behavior of $\tau_{\mathrm{rdip}}(\boldsymbol{r})$ in the interpolation regime makes it difficult to evaluate Markoff's formula [Eq. (10)]. However, we can utilize the substantially different stress magnitudes of the asymptotic regimes. The stress field reaches its highest magnitudes in the two asymptotic regimes near the constituent dislocations that implies a dislocationlike behavior of the tails of the stress distribution function $P^{\mathrm{UHS}}_{\mathrm{rdip}}(\tau)$. In contrast to this, the central part of $P^{\mathrm{UHS}}_{\mathrm{rdip}}(\tau)$ should be ideal dipolelike.

In order to validate the existence of these two regimes, the internal stress distribution of monodisperse dipole configurations was determined numerically. One of the obtained distribution functions is plotted in Fig. 2 together with the theoretically calculated Lorentzian distribution and the asymptotic $1/\tau^3$ formula. It is clear that the distribution function follows the expected behaviors in the corresponding regimes quite well. It is worth noting that the Lorentzian and the asymptotic functions do not contain any fitting parameters, the parameters were calculated analytically.

For describing the entire stress distribution function, one can introduce a suitable interpolating function between the two analytically known asymptotes. However, because of the simpler form of the combination rule given by Eq. (11), it is more useful to perform the interpolation in the Fourier space rather than in the τ space. The rapidly changing central part of $P^{\mathrm{UHS}}_{\mathrm{rdip}}(\tau)$ corresponds to the high frequency regimes of $P^{\mathrm{UHS}}_{\mathrm{rdip}}(q)$, while the decaying tails of $P^{\mathrm{UHS}}_{\mathrm{rdip}}(\tau)$ affect the central part of $P^{\mathrm{UHS}}_{\mathrm{rdip}}(q)$. Consequently, according to Eqs. (16) and (21), we should suppose the asymptotes

$$\ln[P^{\mathrm{UHS}}_{\mathrm{rdip}}(q)] \to \begin{cases} C\rho_{\mathrm{dis}}q^2 \ln\left(\dfrac{|q|}{q_{\mathrm{eff}}}\right) & \text{whenever } |q| \to 0, \\ -D\rho_{\mathrm{rdip}}|q| = -\frac{1}{2}D\rho_{\mathrm{dis}}|q| & \text{whenever } |q| \to \infty, \end{cases} \tag{25}$$

where ρ_{rdip} denotes the planar dipole density. A relatively simple choice can be the following form:

$$\ln[P^{\mathrm{UHS}}_{\mathrm{rdip}}(q)] = Wq^2\left[\ln\left(1+\frac{X}{|q|}\right)+\frac{Y}{q^2+Z}\right], \tag{26}$$

where W, X, Y, and Z are constants. Substituting Eq. (26) into Eq. (25) unambiguously determines the values of W, X, Y, and Z leading to

$$\ln[P^{\mathrm{UHS}}_{\mathrm{rdip}}(q)] = -C\rho_{\mathrm{dis}}q^2\left[\ln\left(1+E\frac{q_{\mathrm{eff}}}{|q|}\right)+\frac{E^2\ln(E)}{2\ln(E)\dfrac{q^2}{q_{\mathrm{eff}}^2}-E^2}\right], \tag{27}$$

where

$$E = D/(2Cq_{\mathrm{eff}}) \tag{28}$$

is a dimensionless constant. [The actual q dependence of the denominator of the second term in expression (27) ensures the homogeneous linearity at large q values.]

According to earlier investigations of Groma and Bakó,[22] for an arbitrary dislocation configuration the value of q_{eff} can be determined from the equation

$$\int d^{+1,-1}_{\mathrm{dis}}(\boldsymbol{r}_1-\boldsymbol{r}_2)\tau_{\mathrm{dis}}(\boldsymbol{r}_1)\tau_{\mathrm{dis}}(\boldsymbol{r}_2)d\boldsymbol{r}_1 d\boldsymbol{r}_2 = \rho_{\mathrm{dis}}\ln\left(\frac{q_{\mathrm{eff}}}{R_c}\right), \tag{29}$$

where $d^{+1,-1}_{\mathrm{dis}}$ is the pair correlation function between dislocations with sign +1 and −1 and R_c denotes the crystal size. However, the analytical expression for $d^{+1,-1}_{\mathrm{dis}}$ is unknown and available numerical data are not precise enough to reliably evaluate q_{eff}. Instead of these, the value of q_{eff} has been obtained numerically by fitting the asymptotes in Eq. (25) to numerical simulations of the stress distribution function in UHS real dipole systems (see Fig. 3 for an example). For 45° edge dislocation dipoles

$$q_{\mathrm{eff}} = \frac{Q}{G}|\boldsymbol{p}|, \quad Q = 5 \pm 2. \tag{30}$$

The proportionality between q_{eff} and $|\boldsymbol{p}|$ is not surprising since for relatively narrow dipoles $|\boldsymbol{p}|$ is the dominating length scale in the given dislocation configuration. Substituting Eq. (30) into Eq. (28) gives $E=0.53\pm0.2$. According to Fig. 3, the interpolation function given in Eq. (27) describes the numerical data with high accuracy.

D. Disperse real dipoles

Real relaxed dislocation configurations contain dipoles with different sizes. Let us denote the probability distribution of dipole sizes by $\mathcal{P}(p)$ where the notation $p=|\boldsymbol{p}|$ is used. The system can be decomposed into UHS arrangements of monodisperse dipoles. Applying the combination rule (11), the stress distribution function of the entire system can be expressed as

$$\ln[P^{\mathrm{UHS}}_{\mathrm{rdip,distr}}(q)] = \int_0^\infty \mathcal{P}(p)\ln[P^{\mathrm{UHS}}_{\mathrm{rdip}}(q,p)]dp, \tag{31}$$

where $\ln[P^{\mathrm{UHS}}_{\mathrm{rdip}}(q,p)]$ denotes the stress distribution of real dipoles given by Eq. (27) with the dipole size dependence explicitly written out.

Equation (31) can be used to calculate the contribution of the dipoles to the stress distribution function of 2D relaxed dislocation systems. To establish the dipole size distribution of relaxed systems, relaxed dislocation configurations like the one in Fig. 1 were analyzed. For each dislocation, the distance of the nearest dislocation of opposite sign was computed. $\mathcal{P}(p)$ was approximated by the distribution of these distances that is reasonable for distances less than the average dislocation distance $1/\sqrt{\rho_{\mathrm{dis}}}$. During relaxation, $\mathcal{P}(p)$ was found to converge to an exponential distribution

$$\mathcal{P}_{\mathrm{relax}}(p) = \frac{1}{p_0}\mathrm{e}^{-(p/p_0)} \quad \text{with } p_0 \approx \frac{0.5}{\sqrt{\rho_{\mathrm{dis}}}} \tag{32}$$

(see Fig. 4). This is consistent with the analysis of Zaiser,

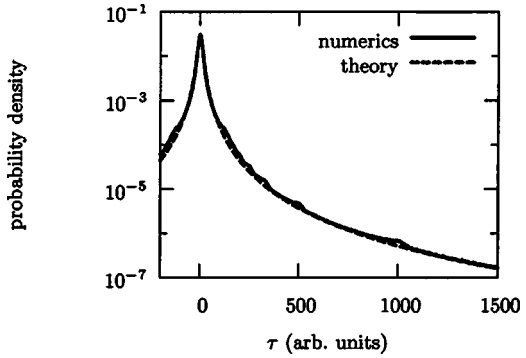

FIG. 3. The numerically obtained stress distribution function shown in Fig. 2 and the interpolating function between the analytically known asymptotes at $|\tau|\to 0$ and $|\tau|\to\infty$ [Eq. (27)].

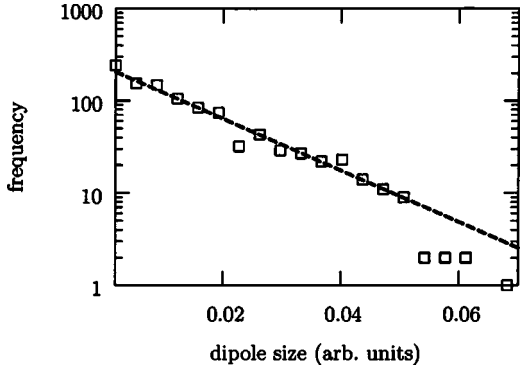

FIG. 4. Dipole size histogram of the relaxed dislocation configuration depicted in Fig. 1. Dotted line: exponential decay fit.

Miguel, and Groma[23] showing that only a faster than algebraic decay of the pair correlation functions is self-consistent in equilibrium dislocation systems.

Substituting the relaxed dipole size distribution in Eq. (32) into Eq. (31) gives

$$\ln[P^{\mathrm{UHS}}_{\mathrm{rdip,distr}}(q)] = -C\rho_{\mathrm{dis}}q^2\left\{-\mathrm{e}^{|q|/q_1}\mathrm{Ei}\left(-\frac{|q|}{q_1}\right)\right.$$
$$-\ln(E)\left[1+\frac{|q|}{q_2}\cos\left(\frac{|q|}{q_2}\right)\mathrm{si}\left(\frac{|q|}{q_2}\right)\right.$$
$$\left.\left.-\sin\left(\frac{|q|}{q_2}\right)\mathrm{Ci}\left(\frac{|q|}{q_2}\right)\right]\right\}, \tag{33}$$

where $q_1=EQp_0$, $q_2=EQp_0/\sqrt{-2\ln(E)}=q_1/\sqrt{-2\ln(E)}$ and Ei, si, and Ci denote the exponential, sine, and cosine integral functions,[27] respectively. In fact, Eq. (33) is effectively an interpolation between the two regimes given by Eq. (25). For certain applications, Eq. (27) can also be applied with appropriately averaged values for D and q_{eff}.

E. Dislocation walls

Besides dipoles, relaxed 2D dislocation configurations contain walls. As a prototype for walls, let us consider a straight, infinitely long wall parallel to the y axis made up of edge dislocations at a distance h having Burgers vectors $s\boldsymbol{b}$ parallel to the x axis. Near the wall, i.e., if $|x|\ll h$, the stress field of the infinite wall is dominated by the stress field of a few nearby dislocations. On the other hand, if $|x|\gg h$, the asymptotic behavior of the stress field can be given as

$$\tau^s_{\mathrm{iwall}}(\boldsymbol{r}) = s\tau_{\mathrm{iwall}}(\boldsymbol{r}) = s4\pi^2\frac{Gb}{h^2}|x|\mathrm{e}^{-2\pi\frac{|x|}{h}}\cos\left(-2\pi\frac{y}{h}\right) \tag{34}$$

(see Landau and Lifshitz[25]). These two asymptotic regimes can be treated similarly to the case of real dipoles described above. As a first step, we calculate the stress distribution function of an idealized wall that generates a stress field described by Eq. (34). The effect of the near stress field is incorporated in a similar way as for real dipoles.

By substituting Eq. (34) into Eq. (10) one obtains for the stress distribution of UHS ideal wall configurations

$$\ln[P^{\mathrm{UHS}}_{\mathrm{iwall}}(q)] = -\frac{\eta_{\mathrm{iwall}}}{h}\int_0^h dy\int_{-\infty}^{\infty}dx$$
$$\times\left\{1-\cos\left[q4\pi^2\frac{Gb}{h^2}|x|\mathrm{e}^{-2\pi|x|/h}\right.\right.$$
$$\left.\left.\times\cos\left(-2\pi\frac{y}{h}\right)\right]\right\}, \tag{35}$$

where η_{iwall} is the line density of ideal walls. With this, the density of dislocations in the walls can be given as η_{iwall}/h. After introducing the new integration variables $\alpha=2\pi x/h$ and $\beta=q2\pi bG\alpha\mathrm{e}^{-\alpha}\cos(-2\pi y/h)/h$, the integral with respect to β can be performed, leading to

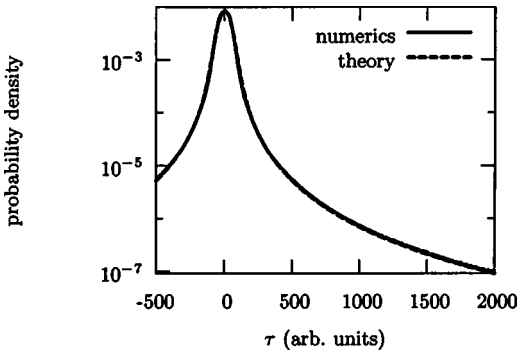

FIG. 5. Numerically obtained stress distribution function of the relaxed dislocation configuration depicted in Fig. 1 and the theoretical stress distribution function described in Sec. III F. Note that the two curves almost fully overlap.

$$\ln[P^{\mathrm{UHS}}_{\mathrm{iwall}}(q)] = -\frac{\eta_{\mathrm{iwall}}h^2}{\pi h}\int_0^{\infty}\left[1-J_0\left(q\frac{2\pi Gb}{h}\alpha\mathrm{e}^{-\alpha}\right)\right]d\alpha, \tag{36}$$

where J_0 is the Bessel function of the first order.[27] For typical values of G, b, and h, the integrand $(1-J_0)$ is well approximated by the first nonvanishing term of its Taylor series around 0, yielding

$$\ln[P^{\mathrm{UHS}}_{\mathrm{iwall}}(q)] = -\pi\frac{\eta_{\mathrm{iwall}}}{h}\left(\frac{Gb}{2}\right)^2q^2. \tag{37}$$

Thus, the stress distribution of an ideal wall is *Gaussian* with a standard deviation of $(\pi/2)\eta_{\mathrm{iwall}}(Gb)^2/2$.

F. Relaxed dislocation configurations

As it was mentioned above, relaxed 2D configurations are made up of two structures, dipoles and walls. We measured the frequency of signs of the nearest neighbors of dislocations. In relaxed configurations, $76\pm1\%$ was obtained for the frequency of opposite sign neighbors, independent of the dislocation density.

According to the results explained above, one can compose the Fourier transform of the stress distribution function of relaxed configurations in the following way. At small q, it starts with a dislocationlike part [see Eq. (16)] coming from both dipoles and walls, containing the total dislocation density ρ_{dis}. At higher q values, it has a dipole part [see Eq. (33)] with an apparent D value 0.76 times smaller than the D value given by Eq. (22). The appearance of a relatively small number of walls can be well approximated by introducing an apparent q_{eff} leading to a Gaussian contribution. The standard deviation corresponding to this Gaussian correction needs to be determined numerically.

One can compare the theoretical stress distribution function constructed above to a numerically obtained stress distribution curve in Fig. 5. It can be seen that the theoretical function satisfactorily describes the numerical curve. One can conclude from this that the entire stress distribution function of relaxed dislocation configurations can be described taking only dislocation pair correlations into account and

omitting all higher order correlations. Numerical calculations have also shown that the stress distribution function of relaxed dislocation configurations depends only on one parameter, the dislocation density.

IV. CONCLUSIONS

The probability distribution of the internal shear stress generated by systems of straight parallel edge dislocations of a common slip system was investigated. The following results have been obtained:

(1) The stress distribution function of uncorrelated, homogeneous, and symmetrical to the sign exchange configurations of dipoles was described as an interpolation between the analytically known Lorentzian asymptote at small and inverse cubic decay at large stresses. The correlation length parameter, that is relatively complicated to calculate analytically, was determined from numerical simulations.

(2) The central part of the stress distribution of straight infinite walls was shown to be of Gaussian-type.

(3) The dipole size distribution of relaxed configurations was numerically shown to be exponential.

(4) The stress distribution function of relaxed configurations was described in terms of uncorrelated sets of perfect dipoles and walls. By numerically fitting the unknown standard deviation of the Gaussian contribution of walls, a distribution function accurate enough for stochastic dislocation dynamics simulations was obtained.

It is worth mentioning that the above considerations are also applicable to other types of pointlike objects generating a $1/r$ type field like e.g., vortices in fluids (see Chavanis and Sire[28]) or dislocations appearing in vortex lattices in type II superconductors studied by Miguel and Zapperi.[29]

ACKNOWLEDGMENTS

Financial support of the Hungarian Scientific Research Fund (OTKA) under Contract No. T 043519 and of the European Community's Human Potential Programme under Contract No. HPRN-CT-2002-00198, [DEFINO] is gratefully acknowledged.

*Electronic address: csikor@metal.elte.hu

[1] D. L. Holt, J. Appl. Phys. **41**, 3179 (1970).
[2] D. Walgraef and E. C. Aifantis, J. Appl. Phys. **15**, 688 (1985).
[3] P. Hähner, Acta Mater. **44**, 2345 (1996).
[4] J. Kratochvíl and R. Sedláček, Phys. Rev. B **67**, 094105 (2003).
[5] I. Groma, F. F. Csikor, and M. Zaiser, Acta Mater. **51**, 1271 (2003).
[6] A. Gullouglu, D. Srolovity, R. LeSar, and P. Lomdahl, Scr. Metall. **23**, 1347 (1989).
[7] R. J. Amodeo and N. M. Ghoniem, Phys. Rev. B **41**, 6958 (1989).
[8] A. N. Gullouglu and C. S. Hartley, Modell. Simul. Mater. Sci. Eng. **1**, 1 (1992).
[9] L. P. Kubin and G. R. Canova, Scr. Metall. Mater. **27**, 957 (1992).
[10] B. Devincre and M. Condat, Acta Metall. Mater. **40**, 2629 (1992).
[11] V. A. Lubarda, J. A. Blume, and A. Needleman, Acta Metall. Mater. **41**, 625 (1993).
[12] I. Groma and G. S. Pawley, Philos. Mag. A **67**, 1459 (1993).
[13] Y. Bréchet, G. R. Canova, and L. P. Kubin, Scr. Metall. Mater. **29**, 1165 (1993).
[14] H. H. M. Cleveringa, E. van der Giessen, and A. Needleman, Acta Mater. **45**, 3163 (1997).
[15] E. C. Aifantis, J. Eng. Mater. Technol. **106**, 326 (1984).
[16] N. A. Fleck and J. W. Hutchinson, Adv. Appl. Mech. **33**, 295 (1997).
[17] J. Y. Shu and N. A. Fleck, J. Mech. Phys. Solids **47**, 297 (1999).
[18] M. E. Gurtin, J. Mech. Phys. Solids **50**, 5 (2002).
[19] B. Svendsen, J. Mech. Phys. Solids **50**, 1297 (2002).
[20] I. Groma, Phys. Rev. B **57**, 7535 (1998).
[21] M. Zaiser and A. Seeger, in *Dislocations in Solids*, edited by F. N. R. Nabarro and M. S. Duesbery (North-Holland, Amsterdam, 2002), Vol. 11.
[22] I. Groma and B. Bakó, Phys. Rev. B **58**, 2969 (1998).
[23] M. Zaiser, M.-C. Miguel, and I. Groma, Phys. Rev. B **64**, 224102 (2001).
[24] S. Chandrasekhar, Rev. Mod. Phys. **15**, 8 (1943).
[25] L. D. Landau and E. M. Lifshitz, *Theory of Elasticity, Vol. 7 in Course in Theoretical Physics*, 3rd ed. (Pergamon, Oxford, 1986).
[26] M. Krivoglaz, *Theory of X-Ray and Thermal Neutron Scattering by Real Crystals* (Plenum, New York, 1969).
[27] M. Abramowitz and I. A. Stegun, *Handbook of Mathematical Functions* (Dover, New York, 1965).
[28] P. H. Chavanis and C. Sire, Phys. Rev. E **62**, 490 (2000).
[29] M.-C. Miguel and S. Zapperi, Nat. Mater. **2**, 477 (2003).
[30] The $1/r$ behavior of the elastic stress field of dislocations breaks down at a few Burgers vectors from the dislocation line. However, the annihilation distance, which refers to the smallest dipole size, is usually an order of magnitude larger than that. This means that there exists a region with a $1/r$ stress field around each dislocation line in all physically reasonable dislocation configurations, which implies that the stress distribution function always has a noticeable dislocationlike tail at high stresses up to a certain stress determined by the dislocation core radius.